OSSE Upper Limits to Pulsar Gamma-Ray Emission

P. C. Schroeder, M. P. Ulmer, S. M. Matz, D. A. Grabelsky, and W. R. Purcell

Department of Physics and Astronomy, Northwestern University, Evanston, IL 60208-3112

J. E. Grove, W. N. Johnson, R. L. Kinzer, J. D. Kurfess, and M. S. Strickman

Code 7650, E. O. Hulburt Center for Space Research, Naval Research Laboratory,
Washington, DC 20375

G. V. Jung[1]

Universities Space Research Association, Washington, DC

Received 30 September 1994; accepted ____________________

---

[1] Postal address, Code 7650, Naval Research Lab, Washington, DC 20375

Report Documentation Page					*Form Approved* *OMB No. 0704-0188*	

1. REPORT DATE **1994**	2. REPORT TYPE	3. DATES COVERED **00-00-1994 to 00-00-1994**
4. TITLE AND SUBTITLE **OSSE Upper Limits to Pulsar Gamma-Ray Emission**		5a. CONTRACT NUMBER 5b. GRANT NUMBER 5c. PROGRAM ELEMENT NUMBER
6. AUTHOR(S)		5d. PROJECT NUMBER 5e. TASK NUMBER 5f. WORK UNIT NUMBER
7. PERFORMING ORGANIZATION NAME(S) AND ADDRESS(ES) **Naval Research Laboratory,Code 7650,4555 Overlook Avenue, SW,Washington,DC,20375**		8. PERFORMING ORGANIZATION REPORT NUMBER
9. SPONSORING/MONITORING AGENCY NAME(S) AND ADDRESS(ES)		10. SPONSOR/MONITOR’S ACRONYM(S) 11. SPONSOR/MONITOR’S REPORT NUMBER(S)

12. DISTRIBUTION/AVAILABILITY STATEMENT
Approved for public release; distribution unlimited

13. SUPPLEMENTARY NOTES

14. ABSTRACT

15. SUBJECT TERMS

16. SECURITY CLASSIFICATION OF:			17. LIMITATION OF ABSTRACT	18. NUMBER OF PAGES	19a. NAME OF RESPONSIBLE PERSON
a. REPORT **unclassified**	b. ABSTRACT **unclassified**	c. THIS PAGE **unclassified**		**27**	

ABSTRACT

We present upper limits from CGRO *Oriented Scintillation Spectrometer Experiment* (OSSE) observations of pulsars and a summary of pulsar observations made with the *Compton Gamma-Ray Observatory* (CGRO). We also report an upper limit to phase-averaged emission for the globular cluster 47 Tuc which is thought to contain many millisecond pulsars. The 2σ upper limit is 3×10^{-5} photons cm^{-2} s^{-1} keV^{-1} in the 50–150 keV energy range. The best predictor of a pulsar having a detectable gamma-ray emission appears to be the X-ray luminosities observed by the Röntgen Satellite (ROSAT) ($\sim$ 0.1–2.4 keV) or the EINSTEIN Satellite ($\sim$ 0.1–4.0 keV). We compare the gamma-ray data to models related to the inferred magnetic field, the spin down rate, and/or the frequency. Apparent correlations indicated by the pulsars detected by OSSE and the CGRO *Energetic Gamma Ray Experiment Telescope* (EGRET) have counter-examples in all cases.

1. INTRODUCTION

The gamma-ray study of pulsars is important not only because it provides insights into the physics of pulsars but because gamma rays are known to be the dominant form of radiative energy loss for several isolated pulsars and may dominate the energy loss of many more. Therefore, if we are going to understand the energetics of pulsars, it is necessary to obtain gamma-ray observations of pulsars. To date, there have been six reported detections of gamma-ray pulsars with the *Compton Gamma-Ray Observatory* (CGRO). The EGRET and COMPTEL teams have also obtained upper limits to gamma-ray fluxes for a number of pulsars. The reader is referred to Thompson et al. (1994), and Fierro et al. (1994), for the latest EGRET upper limit results. The COMPTEL upper limits are in preparation (Carramiñana et al. 1994).

For over three years, the *Oriented Scintillation Spectrometer Experiment* (OSSE) on CGRO has collected data from many known radio and X-ray pulsars. Five pulsars (Crab, Vela, PSR B1706−44, PSR B1055−52, and Geminga) have been detected by the CGRO Energetic Gamma-Ray Experiment Telescope (EGRET), and three (Crab, Vela, and PSR B1509−58) have been detected by OSSE (cf. Ulmer 1994; Matz et al. 1994; Strickman et al. 1993). Apparent trends that relate the gamma-ray luminosity to other pulsar characteristics have been identified (Ulmer 1994). Here we present OSSE upper limits on fifteen additional pulsars. This work extends the EGRET and COMPTEL results to much lower energies and provides a valuable bridge between gamma-ray and X-ray studies of pulsars. We discuss the consequences of these upper limits for gamma-ray emission from isolated pulsars. Similar conclusions have been reached by Thompson et al. (1994), and Fierro et al. (1994).

2. OBSERVATIONS

The Oriented Scintillation Spectrometer Experiment is one of four gamma-ray instruments on the *Compton Gamma Ray Observatory* (Johnson et al. 1993; Ulmer et al. 1993). OSSE consists of 4 identical NaI(Tl)/CsI(Na) phoswich detectors with sensitivity in the .05–10 MeV energy range. The field of view of each detector is $11.4^\circ \times 3.8^\circ$ (FWHM response), defined by a tungsten slat collimator. Each detector can be independently rotated about a fixed direction which is parallel to the long direction of the collimator (and the spacecraft y-axis). Energy losses in each phoswich detector are measured and recorded for later transmission to the ground, along with instrument configuration information and other housekeeping data.

For typical spectral observations, detectors alternately observe source and background positions roughly every two minutes in order to obtain local background measurements. For analysis of pulsed emission, however, only the on-source positions are used. OSSE pulsar modes permit transmission of time-tagged gamma-ray energy losses. Because the entire event stream for all four detectors cannot be accommodated in OSSE's portion of the satellite telemetry, the pulsar processing includes event selection and compression for telemetry formatting. Up to eight energy-band definitions may be included in the transmitted pulsar data. These energy bands, as well as the rest of the pulsar data collection configuration, can be defined by OSSE mission operations activities and uploaded to the instrument via command. The pulsar data acquisition can therefore be optimized to the specific observing strategy and energy range of particular interest, while limiting the event rate to that which can be accommodated by the OSSE telemetry.

Gamma-ray events qualified as being in one of these eight energy bands are processed onboard in one of two modes: (1) event-by-event (EBE) mode, where selected events are time-tagged, and both energy loss and arrival time at the spacecraft are transmitted in the telemetry; or (2) pulsar rate mode, where high time resolution rate samples are taken in each of the eight energy bands.

The EBE mode data provide the highest time resolution, and are therefore suited for the study of fast pulsars. Events are time-tagged with a resolution selectable from either 1/8 or 1 milliseconds. In this mode, spacecraft arrival times, detector identifications, and encoded energy losses are transmitted. At the highest resolution, the telemetry bandwidth supports a maximum event rate of $\sim$ 290 events per second, and the maximum event rate for 1 ms is $\sim$ 20% lower. Regardless of the resolution selected for telemetry, gamma-ray events that pass the instrument anti-coincidence criteria (valid gamma-ray events) are registered on board the spacecraft with 1/8 millisecond ticks, relative to the UTC time marking the beginning of each standard 2.048 s data packet. Event timing precision in the telemetry stream may then be truncated, depending upon the selected resolution.

The pulsar rate mode can accommodate a much higher event rate, but at the expense of spectral resolution. This mode records the number of events in each of the defined energy bands at a specified sample frequency. The highest sample rate in this mode provides a resolution of 4 milliseconds. Sample times from 4 msec to 512 msec can be selected. In this mode OSSE can achieve its best sensitivity to a continuum flux.

In our observations, the pulsar data acquisition energy ranges were set to cover that portion of the spectrum where we judged OSSE would have the best chance of detecting a given pulsar. Further, we adjusted the energy bandwidth so that the telemetry could accommodate (with a dead time loss of $\leq$ 20%) the detector background counting rate within that energy range (cf. Johnson et al. 1993). Table 1 provides a summary of the observations.

While we observed many of these pulsars over a long period of time, most of them were not the primary objects of observation. Consequently, only a fraction of the elapsed time of each observation was actually spent observing these pulsars. Also, the pulsars were often not in the center of the field of view so a geometric factor had to be introduced to reflect the reduced effective area of each detector. So, while a pulsar may have been observed over a two week time span, conditions may not have been optimal for its detection. OSSE has an on-going project to observe pulsars, and in this paper, we report the results of observations made through 1993 March 9.

3. ANALYSIS AND RESULTS

OSSE has spent a significant amount of time observing fifteen pulsars, most of which were expected to be good candidates for detection in low-energy gamma rays because of their relatively high $\dot{E}/d^2$ ratios ($\dot{E}/d^2 > 10^{34}$ erg s^{-1} kpc^{-2}) or their detection in high-energy gamma rays by EGRET, where $\dot{E}$ denotes the inferred rotational energy loss assuming a moment of inertia of 10^{45} g-cm^2 and d is the distance to the pulsar (cf. Taylor, Manchester, & Lyne 1993). Data taken during the observation of each pulsar were folded using the appropriate radio ephemeris (Taylor et al. 1992), except in the case of Geminga where the gamma-ray ephemeris was used (Mayer-Hasselwander et al. 1994).

The epoch-folded data were searched for evidence of a pulsed signal by using a χ^2 test of the fit to a constant intensity. Since the data were binned in 32 channels, a value of $\chi^2 \gtrsim 50$ would have been judged significant at the 2σ level. One pulsar, PSR B1929+10, had $\chi^2 = 51$ which was considered marginally significant.

We also fitted each epoch-folded data set to circular normal functions with full width half maxima of both 0.6 and 0.3 cycles. These functions were of the form:

$$f(\phi) = ae^{b\cos[2\pi(\phi-c)]} + d \tag{1}$$

where a is proportional to the peak of the distribution, b is a measure of its compactness, c gives the phase of the peak of the distribution, and d represents a constant background.

The statistical properties of this function were explored by von Mises (cf. Johnson & Katz 1970). The compactness parameter b is related to the full width half maximum (FWHM) of the peak by the equation:

$$\text{FWHM} = \pi^{-1} \arccos[b^{-1}(\ln[0.5(e^{b} - e^{-b})])] \tag{2}$$

Therefore, the values of b corresponding to full width half maxima of 0.6 and 0.3 cycles are 0.73 and 1.8, respectively. Because the function in Equation 1 is circular, we could search for a signal at any phase in the data set. A statistically significant result would be one in which the value of a was greater than twice the uncertainty to a. Both PSR B1929+10 and PSR B2334+61 fit this criterion, each with values of a as high as 2.7 times the uncertainty to a, an occurrence with an associated probability of $\sim 0.3\%$. But, given that there were fifteen pulsars in our sample, the effective probability of this occurrence is increased to $\sim 2\%$. We would expect this test to detect pulsars whose light curves are single-peaked. Crab-like pulsars with double-peaked light curves are more easily detected with the χ^2 test.

To verify that the fitting procedure had not missed a narrow peak in the case of the circular normal functions, visual inspections of the data sets of all the pulsars were also conducted. We concluded that no pulsars were detected in this survey.

We did not initially apply the Z_m^2 or H tests (Buccheri et al. 1983; De Jager et al. 1989) to our data to search for evidence of pulsed emission because our data sets contained sufficient counts so that binning the data to 32 or more phase bins per light curve produced well over 1000 counts per bin (i.e. Gaussian statistics apply). Hence, the data did not require the use of the Z_m^2 or H tests, whose only real advantage for pulsars with known ephemerides is that no binning is required (Thompson et al. 1994; D. J. Thompson 1994, private communication; J. P. Finley 1994, private communication). For completeness, however, we specifically applied the Z_2^2 test to Crab pulsar test sets comprised of 2-minute integrations. The 2-minute integrations were small enough to produce an $\sim 3\sigma$ signal as found by the χ^2 test. The Z_2^2 test was slightly less sensitive, finding the result only significant at the 90% confidence level. Thus, we specifically demonstrated that the χ^2 test is sufficient for our purposes and we proceed accordingly.

Since we could find no statistically significant pulsed signal from any of these pulsars, we computed the upper limits using the prescription (Ulmer et al. 1991):

$$\sigma = \frac{f^{1/2} C_t^{1/2}}{AT\Delta E}, \tag{3}$$

where

$$f = \frac{\beta}{1-\beta}. \tag{4}$$

In this formula, C_t is the total number of counts, A is the effective detector area, T is the total exposure time, and ΔE is the size of the energy window. We chose the value of the pulsar duty cycle β to be 0.5. This is a typical value for known gamma-ray pulsars (cf. Ulmer 1994), and this formalism allows the reader to easily adjust the upper limits to any other assumed value of β. To check that the upper limits that were derived in this manner were not overly conservative (too high) or optimistic (too low), we computed 2σ upper limits from the best fit circular normal functions with full width half maxima constrained to 0.6 and 0.3 by assuming a signal with a peak area equal to twice the uncertainty to the peak area derived for that pulsar. Typically, the 2σ limits from the fit with a FWHM of 0.3 were a factor of ~ 0.6 times the limit derived from Equation 3. The limits from the fit with a FWHM of 0.6 were a factor of ~ 1.1 times the derived limits. The total variance of the upper limits from the fits were 0.24–4.0 times the upper limits derived from Equation 3. We can conclude that the upper limits derived using Equations 3 and 4 are comparable to those derived from other methods and that they are neither too optimistic nor too conservative. In Table 2 we present the 2σ upper limits to the phase averaged flux, using Equations 3 and 4. Because the observations of many of the pulsars involved disparate energy ranges, we report only the lowest upper limit that can be derived for each pulsar. This corresponded to the lowest energy range, where OSSE has the best sensitivity.

In addition to the standard epoch-folding analysis of individual pulsars, we also performed a search for DC emission from the globular cluster 47 Tuc, which is thought to contain many pulsars (see §4.3). The observations of 47 Tuc took place during observations of the known (cf. Reynolds et al. 1993) X-ray binary SMC X−1 which were performed from 1993 May 8 to 1993 May 13 and from 1993 June 3 to 1993 June 14. These were normal offset-pointed observations of SMC X−1 in which on-source observations were alternated with background observations offset from the source position by ± 4.5 degrees. During these observations, 47 Tuc was included in the SMC X−1 source field and in one of the background fields; the second background field was free of any known hard X-ray source. The analysis for the 47 Tuc observation was performed using the standard background subtraction and data screening techniques described by Johnson et al. (1993; see also Osako et al. 1994). The observed counting rate was converted to a photon flux using the instrument response for the location of 47 Tuc in the source and background fields and assuming an E^{-2} spectral shape. No significant emission was detected from 47 Tuc. The 2σ upper limit is 3×10^{-5} photons cm^{-2} s^{-1} keV^{-1} in the 50–150 keV energy range. As discussed in §4.3, this limit is ~ 5 times lower than the previously reported result (Barret et al. 1993).

4. DISCUSSION

4.1. Luminosity Upper Limits

Under the assumption that the pulsars we observed were like those pulsars most easily detected by OSSE (the Crab pulsar and PSR B1509−58), we have assumed a $1/E^2$ spectral shape to derive the upper limits for all the pulsars in Table 2. For pulsars such as PSR B1706−44 and Geminga, $1/E^2$ upper limits underestimate the 100 keV to 1 GeV energy fluxes by factors of 10–100. But, if most pulsars had flat spectra like Geminga and PSR B1706−44, and their spectra extrapolated to the ~ 100 keV energy range at flux levels just below the OSSE sensitivity, they would have been easily detected by EGRET. In §4.2 we describe how we treated the pulsars detected by EGRET that were observed but not detected by OSSE (PSR B1706−44 and Geminga).

We made an annotation next to those pulsars in Table 2 which we have not plotted at their observed upper limits. The upper limits set by OSSE of these pulsars were higher than the total estimated rotational energy loss. Therefore, for purposes of presentation, we used 90% of the rotational energy loss as a conservative upper limit. Distances to the pulsars were taken from the Taylor et al. (1993) catalog. These distances were primarily based on a model of Taylor & Cordes (1993) which converts dispersion measure to distance. However, in some instances more data were available, and those pulsars have also been noted in our tables. For the Geminga pulsar, which has not been detected in the radio, we have assumed the distance to be 0.15 kpc [see Thompson et al. (1994), and Halpern & Ruderman (1993), for discussions of the distance estimate]. Further, we assumed the width of the pulsar beam perpendicular to the pulse plane passing through Earth to be 90° (e.g., the flux limits were converted to luminosity limits by multiplying by $2\pi d^2$). It is possible that the beaming angle of gamma-ray emission also varies from pulsar to pulsar.

4.2. Converting Detections to Fluxes

The largest uncertainties based upon measured quantities (as opposed to uncertainties due to assumptions about quantities such as beaming angles) that we used in determining luminosities are due to distance estimates and the extrapolation of pulsar spectra outside the range where they were detected. We have ignored these uncertainties in plotting the upper limits as, on average, the distances should be correct to better than 50% (cf. Taylor et al. 1993), and the assumption of a $1/E^2$ spectral shape also produces fluxes that differ from the true values by $\lesssim$ 50% in the cases of those pulsars easily detected by OSSE such as the Crab and PSR B1509−58. For the detected pulsars, the distance uncertainties dominate, and amount to a factor of two. For these we have combined the uncertainties based on the distance estimates and extrapolations to the spectra in quadrature to produce the resultant uncertainties. We remark that only an upper limit to the pulsed emission has been set for the X-ray flux of PSR B1706−44 (Becker 1994), and further, assumptions in the X-ray spectral shape of PSR B1706−44 can lead to variations of a factor of 10 in its estimated X-ray luminosity. For the pulsed X-ray flux, we have chosen a value equal to half the 2σ upper limit of the pulsed emission multiplied by the total flux for PSR B1706−44, as reported by Becker.

These results are summarized in Tables 3 (CGRO detections) and 4 [selected ROSAT and EINSTEIN detections from Ögelman (1995), and Becker (1994)].

4.3. Comparisons of Upper Limits to Pulsar Characteristics

We use the following model as a framework for comparing ROSAT ($\sim$ 1 keV) observations with OSSE ($\sim$ 100 keV) observations: while particles are accelerated out to produce beams of non-thermal radiation in the form of gamma rays, the particles are also accelerated down onto the neutron star polar cap surface. The particles heat the polar cap regions, and we suggest that the particle flux accelerated upward is proportional to the flux accelerated downward. Thus the soft X-ray ($\sim$ 1 keV) emission from the heating of the polar caps is related to the hard X-ray ($\sim$ 100 keV) emission. The non-thermal emission might also extend to the soft X-ray regime as well. Therefore, we expect a correlation between the $\sim$ 1 keV and $\sim$ 100 keV X-ray fluxes, and for the detections this is the case, as shown in Figure 1. The upper limits are consistent with this trend. However, there is a wide variance in the detected pulsars' properties when measured by the comparison of their $\sim$ 100 keV flux (OSSE energy range) versus their $\sim$ 1 GeV (EGRET energy range) flux: PSR B1509−58 is easily detectable by OSSE but not detectable by EGRET; and the Vela pulsar is easily detectable by EGRET but is detected only weakly by OSSE (and ROSAT).

Next, we compare the OSSE hard X-ray observations with the inferred voltage from the Crab outer-gap model (Cheng et al. 1986). The potential drop is believed to accelerate charged particles to relativistic speeds which, in turn, radiate in the gamma rays. We see in Figure 2 that there may be a correlation between the hard X-ray luminosity and the outer gap potential drop. Our upper limits are again consistent with this trend, but more sensitive results are needed before we can conclude that this outer-gap picture for hard X-ray production is correct.

Notably, no millisecond pulsars have been detected by OSSE or EGRET (Fierro et al. 1994). These upper limits are consistent with the 2σ upper limit derived for the globular cluster 47 Tuc. The upper limit to 47 Tuc of about 3×10^{-5} photons cm^{-2} s^{-1} keV^{-1} in the 50–150 keV energy range corresponds to ~ 0.3 Crab pulsars and is higher than that reported by Barret et al. (1993) by a factor of two. 47 Tuc is thought to contain many millisecond pulsars (cf. Barret et al., and references therein) and is at an estimated distance of 5 kpc [or 4.4 kpc (Storm et al. 1994)]. If we assume there are 100 pulsars in 47 Tuc [at least 11 have been detected (cf. Manchester et al. 1991)], the above limit corresponds to an average millisecond pulsar strength of less than $\sim 3 \times 10^{-3}$ Crab pulsars.

We next turn to a consideration of future prospects in terms of current upper limits and CGRO's sensitivity. For this we have compared in Figure 3 the values of $\dot{E}/d^2$ with the OSSE measurements. Optimistically, OSSE would have detected those pulsars (Geminga and PSR B1706$-$44) with an energy loss flux higher than that of PSR B1509$-$58 (the diamond in Figure 3) and/or those for which the OSSE sensitivity places the upper limits well below the 1% efficiency line (PSR B1951+32, PSR B1929+10, PSR B1046$-$58, PSR B1706$-$44, and Geminga; note the diagonal dashed lines demark the 100% and 1% efficiency loci of the efficiency of converting rotational energy loss into a hard X-ray flux). That PSR 1929+10 gave a $\sim 2\sigma$ signal is tantalizing however. Also, errors in the distance estimates could explain why the energy loss "flux" ($\dot{E}/d^2$) predictor is not a good one.

5. SUMMARY AND CONCLUSIONS

We have not been able to find a set of pulsar characteristics that we can use as a reliable predictor of when a pulsar will be detectable in the hard X-ray/gamma-ray ($\gtrsim 50$ keV) region. The best predictors seem to be: 1) a strong X-ray flux, which predicts that a pulsar is detectable by OSSE if the X-ray flux is brighter than that of the Vela pulsar ($F_x \geq 1.7 \times 10^{-12}$ erg s^{-1} cm^{-2}), 2) an implied outer-gap voltage drop $\gtrsim 5 \times 10^{15}$ volts predicts the pulsar can be detected by OSSE in the hard X-ray (~ 100 keV) range, and 3) a pulsar period $\lesssim 10$ ms, which predicts that a pulsar would not be detectable by OSSE in the hard X-ray range. A possible reason that we have failed to detect these millisecond pulsars is that their magnetic fields are too low to produce gamma-ray emission. Alternatively, if they did "turn on" as gamma-ray emitters, they might radiate their rotational energy away so efficiently that they would not last long enough to be detected as millisecond pulsars. Searches for young rapidly rotating pulsars in systems such as SN1987A may eventually shed more light on the ability of millisecond pulsars to radiate in the hard X-ray/gamma-ray regime. In deriving the luminosities here, we have assumed that the conversion of flux to luminosity was the same for all pulsars, as it is impossible to measure the width of the pulsar beam perpendicular to the plane passing over Earth. This potentially important quantity, as well as others such as the orientation of the magnetic field relative to the spin axis of the pulsar, prevents us from making definitive conclusions about the physical relationship between the gamma-ray emission and other measured properties of pulsars.

6. ACKNOWLEDGEMENTS

We thank the many radio astronomers [cf. the Princeton ftp pulsar data file (Taylor et al. 1992)] responsible for continually monitoring pulsars and posting the relevant ephemerides necessary to make this work possible. We especially thank those with whom we have had personal contact (Z. Arzoumanian, M. Bailes, J. Cordes, J. Foster, V. Kaspi, S. Lundgren, A. Lyne, R. Manchester, D. Nice, and J. Taylor). We also thank W. Becker for communicating his results for PSR B1706−44. We thank the referees for their comments. This work was supported in part by NASA grant DPR S-10987C and a grant from the Aerospace Illinois Space Consortium.

Table 1: SUMMARY OF OBSERVATIONS

Pulsar B	Dates$^{(a)}$	Exposure$^{(b)}$	GF$^{(c)}$	Energies$^{(d)}$	Detectors$^{(e)}$	Ephemeris$^{(f)}$
0114+58	91/06/08 – 91/06/14	2.1E8	0.85	46–290	2	P
	93/02/25 – 93/03/09				2	
Geminga	92/07/16 – 92/08/06	5.0E8	0.99	76–570	4	G
				2000–9900		
0950+08	91/07/26 – 91/08/08	1.6E8	0.61	18–57	2	P
				58–210		
1046−58	91/11/14 – 91/11/28	5.3E7	0.74	47–160	4	A
1702−19	91/07/12 – 91/07/26	2.2E7	0.15	38–85	4	P
	91/12/12 – 91/12/30			37–150	4	
	92/02/20 – 92/03/05			35–56	4	
	92/04/02 – 92/04/23			79–170	4	
1706−44	91/09/05 – 91/09/12	2.5E8	0.38	31–87	4	A
	91/11/07 – 91/11/14			86–190	4	
	92/12/07 – 92/12/22			230–730	2	
1800−21†	91/12/27 – 92/01/10	3.9E7	0.45	36–63	4	P
	92/04/09 – 92/04/23			77–170	4	
	92/12/05 – 93/01/05				4	
1821−24	91/10/10 – 91/10/13	2.5E7	0.53	70–160	2	P
	92/04/09 – 92/04/16			36–74	2	
	92/12/05 – 93/01/08				4	
	93/02/22 – 93/02/25				4	

Pulsar B	Dates[a]	Exposure[b]	GF[c]	Energies[d]	Detectors[e]	Ephemeris[f]
1822−09	91/08/15 – 91/08/21	2.7E8	0.45	64–160	4	P
	91/10/31 – 91/11/07			77–570	4	
	93/01/12 – 93/02/02			2000–9900	4	
1855+09	92/02/06 – 92/02/20	4.3E7	0.61	35–59	4	P
				77–180		
1929+10	92/01/10 – 92/01/23	3.6E8	0.99	30–170	4	P
				220–340		
				430–530		
				780–910		
				990–1100		
				1200–1500		
				2000–9900		
1937+21	91/05/18 – 91/05/30	2.3E8	0.69	77–160	2	J
	92/01/23 – 92/02/06			330–610	4	
				730–1100		
				2000–9800		
1951+32	91/06/06 – 91/06/15	2.1E8	0.75	74–400	4	J, C, Q
	91/11/28 – 91/12/11			1800–4500	2	
	92/12/08 – 92/12/22				4	
1957+20	91/05/16 – 91/05/23	3.0E8	1.00	200–580	1	P
2334+61	92/07/16 – 92/08/06	2.4E7	0.30	76–170	4	P

Notes for Table 1:

† PSR B1800−21 was observed for guest observers S. Lundgren and J. M. Cordes

a. Dates of OSSE observation

b. Net exposure in cm^2 s [product of the total live time of all detectors, the area of a single detector (500 cm^2), and the geometric factor]

c. Geometric factor of the OSSE observation to reflect loss of effective area for off-axis targets

d. Energy range of the OSSE observation in keV

e. Number of detectors used to observe the pulsar

f. Source for ephemeris: A (Kaspi et al. 1994), C (Cordes et al. 1992), G (Mayer-Hasselwander et al. 1994), J (Lyne, Shemar, & Pritchard 1992), P (Arzoumanian, Nice, & Taylor 1992), Q (S. Lundgren 1993, private communication)

Table 2: GAMMA-RAY LUMINOSITY UPPER LIMITS

ID	Pulsar B	$P^{(a)}$	log $\dot{P}^{(b)}$	log $\dot{E}^{(c)}$	B$^{(d)}$	d$^{(e)}$	Energy Band$^{(f)}$	Upper Limits $F_\gamma^{(g)}$	$L_\gamma^{(h)}$
1	0114+58	0.10144	-14.23	35.34	7.76E11	2.12	46–290	1.85E-7	3.0E33
2	Geminga	0.23700	-13.96	34.51	1.61E12	0.15†	76–570	1.61E-8	4.1E30
3	0950+08	0.25307	-15.64	32.75	2.45E11	0.12†	58–210	3.59E-7	1.7E31
4	1046−58	0.12365	-13.02	36.30	3.47E12	2.98	47–160	4.54E-7	8.1E33
5	1702−19	0.29899	-14.38	33.79	1.12E12	1.19	38–85	2.51E-7	3.0E32
6	1706−44	0.10245	-13.03	36.53	3.16E12	1.82	31–87	3.20E-6	7.6E33
7	1800−21	0.13361	-12.87	36.35	4.27E12	3.94	77–170	6.60E-7	3.6E34
8	1821−24	0.00305	-17.79	36.35	2.24E09	5.50†	70–160	1.06E-6	9.6E34
9	1822−09*	0.76897	-13.28	33.66	6.47E12	1.03	64–160	6.78E-7	1.9E33
10	1855+09*	0.00536	-19.75	33.66	3.16E08	1.00†	35–59	3.70E-6	2.0E33
11	1929+10	0.22652	-14.94	33.59	5.13E11	0.17	30–170	1.83E-7	7.3E30
12	1937+21	0.00156	-18.98	36.04	4.07E08	3.58	77–160	2.66E-7	1.1E34
13	1951+32	0.03953	-14.23	36.57	4.90E11	2.50†	74–400	9.62E-8	4.7E33
14	1957+20	0.00161	-19.77	35.20	1.66E08	1.53	200–580	4.53E-7	1.8E34
15	2334+61*	0.49524	-12.72	34.79	9.77E12	2.46	76–170	7.59E-7	1.6E34

Notes for Table 2:

∗ The upper limits for these exceed the estimated total rotational energy loss

† The distances to these pulsars were found using methods other than the Taylor & Cordes (1993) model for converting dispersion measure to distance

a. Pulsar period in units of s

b. Log of the time derivative of the period

c. Log of the rate of rotational energy loss in erg s^{-1}

d. Magnetic field strength in gauss

e. Distance in kpc

f. Energy range of the OSSE observation in keV

g. Gamma-ray flux upper limit for the given energy range in photons cm^{-2} s^{-1} keV^{-1}

h. Gamma-ray luminosity upper limit (50–200 keV) in erg s^{-1}

Table 3: PROPERTIES OF PREVIOUSLY DETECTED PULSARS

Name	$P^{(a)}$	log $\dot{P}^{(b)}$	log $\dot{E}^{(c)}$	B$^{(d)}$	d$^{(e)}$	$F_{\gamma}^{(f)}$	$L_{\gamma}^{(g)}$
Crab	0.03340	-12.38	38.65	3.80E12	2†	3.5E-9	8.4E35
Vela	0.08930	-12.90	36.84	3.39E12	0.5†	8.8E-12	1.3E32
PSR B1509−58	0.15023	-11.81	37.25	1.55E13	4.4†	1.3E-10	1.5E35

Notes for Table 3:

† The distances to these pulsars were found using methods other than the Taylor & Cordes (1993) model for converting dispersion measure to distance

a. Pulsar period in units of s

b. Log of the time derivative of the period

c. Log of the rate of rotational energy loss in erg s^{-1}

d. Magnetic field strength in gauss

e. Distance in kpc

f. Hard X-ray flux, 50–200 keV, in units of erg cm^{-2} s^{-1}

g. Hard X-ray luminosity, 50–200 keV, in units of erg s^{-1}

Table 4: X-RAY PROPERTIES OF SELECTED PULSARS

Name	$F_x^{(a)}$	$L_x^{(b)}$	Experiment$^{(c)}$
Crab	2.7E-9	6.5E35	R
Vela	3.4E-12	2.5E31	R
PSR B1509−58	9.5E-12	1.1E34	R
PSR B1706−44	4.3E-13	8.5E31	R
Geminga	3.3E-13	4.5E29	R
PSR B1951+32	1.3E-12	5.0E32	R
PSR B0950+08	8.4E-14	7.2E28	E
PSR B1929+10	8.4E-14	1.4E29	E

Notes for Table 4:

a. X-ray flux, (0.1–2.4 keV for ROSAT detections, 0.1–4.0 keV for EINSTEIN detections) in units of erg cm^{-2} s^{-1}

b. X-ray luminosity in units of erg s^{-1} for above energy range

c. X-ray experiment (R: ROSAT, E: EINSTEIN)

7. REFERENCES

Arzoumanian, Z., Nice, D., & Taylor, J. H. 1992, GRO/Radio Timing Database, Princeton University

Barret, D., et al. 1993, ApJ, 405, L59

Becker, W. 1994, Ph.D. thesis, Ludwig-Maximilians-Universität, München

Buccheri, R., et al. 1983, A&A, 128, 245

Carramiñana, A., et al. 1994, in preparation

Cheng, K. S., et al. 1986, ApJ, 300, 500

Cordes, J. M., Backer, D. C., Foster, R. S., Weisberg, J. M., & Lundgren, S. 1992, GRO/Radio Timing Database, Princeton University

De Jager, O.C., et al. 1989, A&A, 221, 180

Fierro, J., et al. 1994, ApJ, submitted

Halpern, J. P., & Ruderman, M. 1993, ApJ, 415, 286

Johnson, N. L., & Katz, S. 1970, Continuous Univariate Distributions—2 (New York: Houghton Mifflin)

Johnson, W. N., et al. 1993, ApJS, 86, 693

Kaspi, V. M., Manchester, R. N., Bailes, M., D'Amico, N., & Lyne, A. G. 1994, GRO/Radio Timing Database, Princeton University

Lyne, A. G., Shemar, S. L., & Pritchard, R. S. 1992, GRO/Radio Timing Database, Princeton University

Manchester, R. N., et al. 1991, Nature, 352, 219

Matz, S. M., et al. 1994, ApJ, 434, 288

Mayer-Hasselwander, H. A., et al. 1994, ApJ, 421, 276

Ögelman, H. 1995, in The Lives of Neutron Stars, eds. M. A. Alpar, Ü. Kiziloğlu, & J. van Paradijs (Dordrecht: Kluwer), 101

Osako, C. Y., et al. 1994, ApJ, 435, 181

Reynolds, A. P., Hilditch, R. W., Bell, S. A., & Hill, G. 1993, MNRAS, 261, 337

Storm, J., Nordström, B., Carney, B. W., & Andersen, J. 1994, A&A, in press

Strickman, M. S., et al. 1993, in Compton Gamma-Ray Observatory, ed. M. Friedlander, N. Gehrels, & D. Macomb (New York: AIP), 209

Taylor, J. H., et al. 1992, public database, anonymous login via ftp to puppsr@princeton.edu

Taylor, J. H., & Cordes, J. M. 1993, ApJ, 411, 674

Taylor, J. H., Manchester, R. N., & Lyne, A. G. 1993, ApJS, 88, 529

Thompson, D. J., et al. 1994, ApJ, 436, 229

Ulmer, M. P. 1994, ApJS, 90, 789

Ulmer, M. P., Purcell, W. R., Wheaton W. A., & Mahoney, W. A. 1991, ApJ, 369, 485

Ulmer, M. P., et al. 1993, ApJ, 417, 738

8. FIGURE CAPTIONS

Figure 1: The gamma-ray flux versus X-ray flux. Squares indicate pulsars detected by EGRET, diamonds indicate pulsars detected by OSSE, triangles indicate pulsars detected by both EGRET and OSSE. Upper limits derived in this paper are indicated by arrows. Asterisks indicate upper limits for millisecond pulsars. The key is the same for all subsequent figures. From left to right, the upper limits by ID number are: 3, 11, 2, 6, 13 (see Table 2).

Figure 2: The gamma-ray luminosity versus voltage drop. Key is same as in Fig. 1. From left to right, the upper limits by ID number are: 3, 11, 5, 2, 14, 1, 12, 4, 8, 7, 6, 13 (see Table 2).

Figure 3: The measured gamma-ray flux versus the maximum possible flux based on the total implied rotational energy loss, see text. The key is same as in Fig. 1. From left to right, the upper limits by ID number are: 5, 10, 3, 1, 14, 8, 12, 7, 11, 4, 13, 6, 2 (see Table 2).

Fig. 1.—

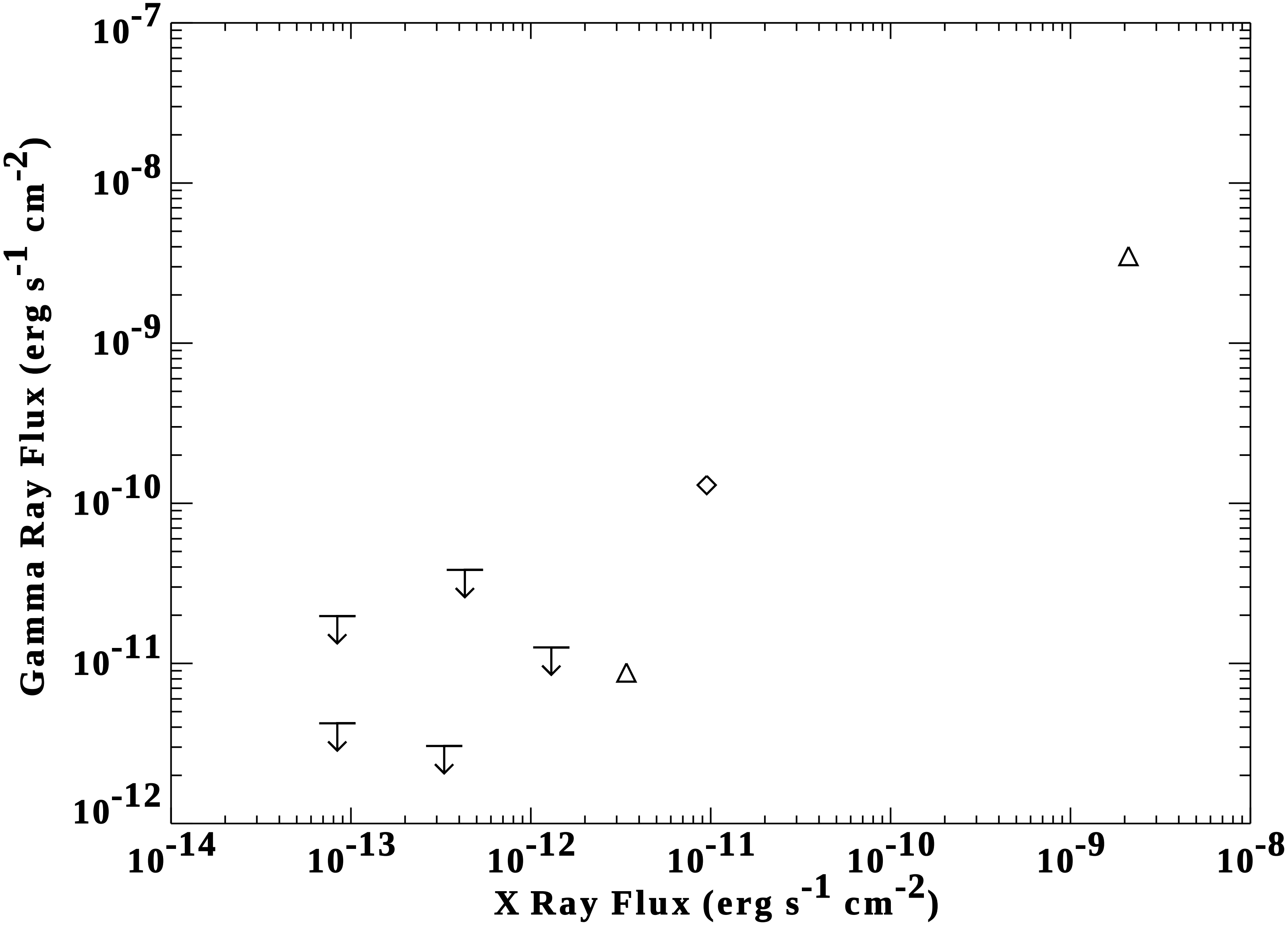

Gamma Ray Flux (erg s^{-1} cm^{-2})
10^{-7}
10^{-8}
10^{-9}
10^{-10}
10^{-11}
10^{-12}
10^{-14}
10^{-13}
10^{-12}
10^{-11}
10^{-10}
10^{-9}
10^{-8}
X Ray Flux (erg s^{-1} cm^{-2})

Fig. 2.—

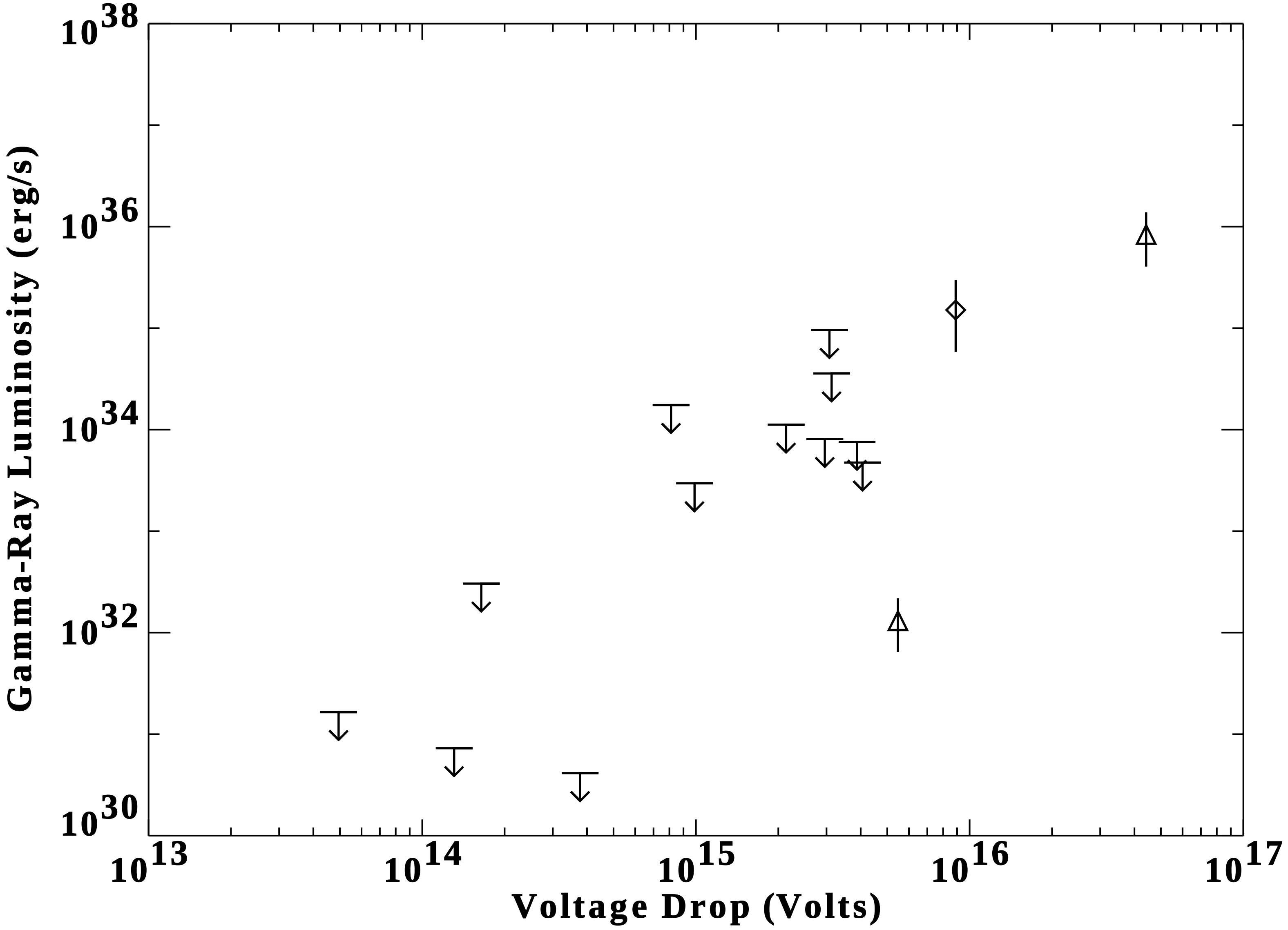
Gamma-Ray Luminosity (erg/s)
10^{38}
10^{36}
10^{34}
10^{32}
10^{30}
10^{13}
10^{14}
10^{15}
10^{16}
10^{17}
Voltage Drop (Volts)

Fig. 3.—

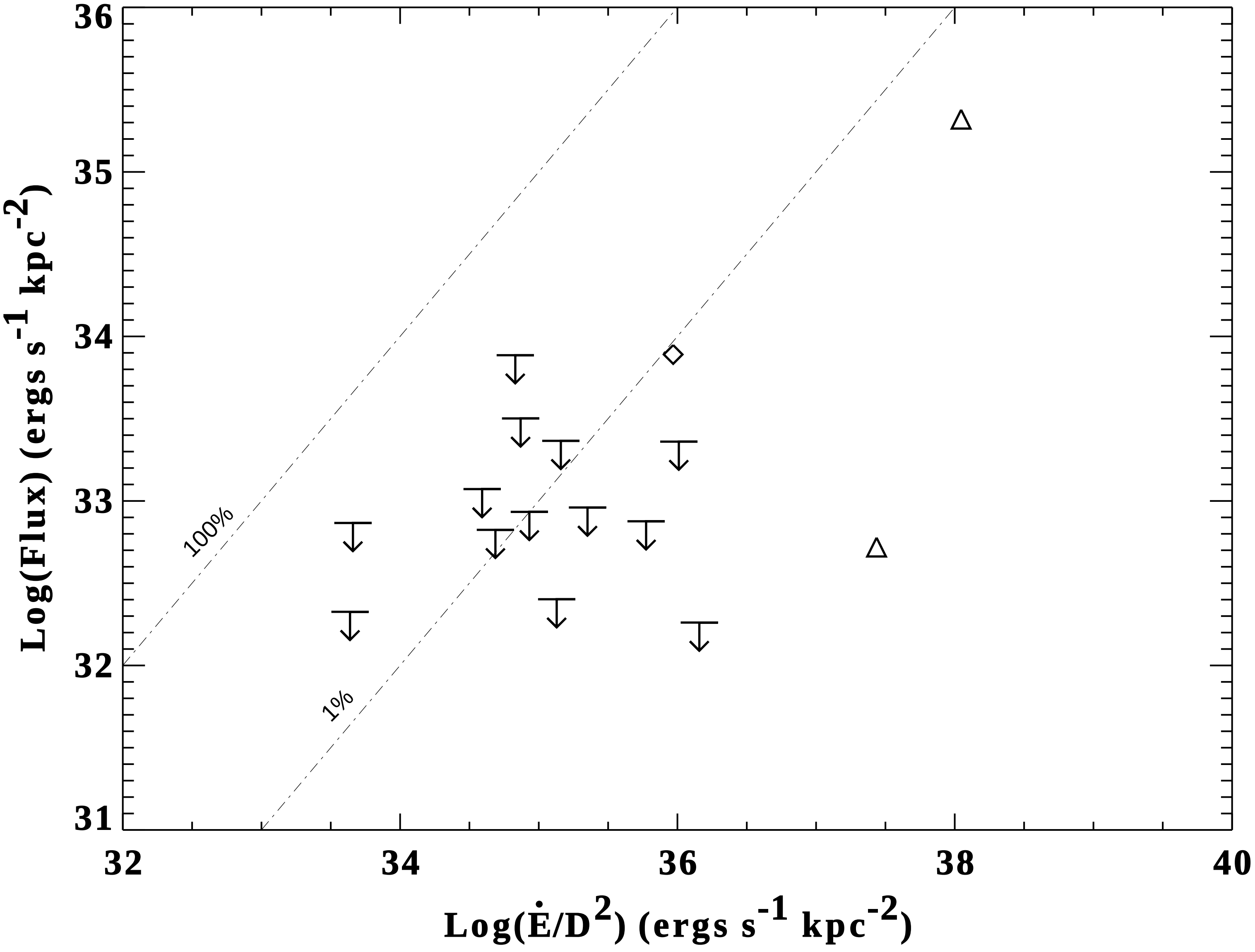

36
35
34
33
32
31
32
34
36
38
40
100%
1%
Log(Flux) (ergs s^{-1} kpc^{-2})
Log($\dot{E}$/D^2) (ergs s^{-1} kpc^{-2})